JOURNAL OF MATERIALS SCIENCE 24 (1989) 1503–1512

Study of Nicalon-based ceramic fibres and powders by EXAFS spectrometry, X-ray diffractometry and some additional methods

C. LAFFON, A. M. FLANK, P. LAGARDE, M. LARIDJANI
LURE, Bât. 209D, 91405 Orsay Cedex, France

R. HAGEGE
Institut textile de France, 35, rue des Abondances, 92100-Boulogne, France

P. OLRY, J. COTTERET
Société Européenne de Propulsion, 33160-St Medard, en Jalles, France

J. DIXMIER
Laboratoire de Physique des Solides, 1, place A. Briand, 92195-Meudon, France

J. L. MIQUEL, H. HOMMEL, A. P. LEGRAND
Laboratoire de Physique Quantique de l'ESPCI, U.A. 421, 10 Rue Vauquelin, 75005-Paris, France

The Nicalon SiC-based ceramic fibres and their precursors have been investigated by complementary techniques: EXAFS, WAXS, ESCA and NMR. For SiC–Nicalon fibres, an alternative model is proposed based on a microcrystalline structure where pure β-SiC is embedded in a continuum of tetrahedral SiC_xO_y ($x + y = 4$). We have found that the inorganic material skeleton is already contained in the carbon and silicon structure of the polymer precursor.

1. Introduction

Silicon carbide (SiC) fibres are among the "high performance fibres", and were designed and developed in order to reinforce various kinds of matrices, e.g. polymeric, metallic or ceramic-including SiC matrices; such "new composite materials" should soon play an active part (and they indeed already do so) in the aerospace industry and perhaps also in the automotive industry. They were introduced onto the market around 1980 by the Japanese Company Nippon Carbon; this company is, up to now, as far as we know, the only one to propose, under the trademark "Nicalon" a continuous SiC multifilament, which is prepared according to the principles patented some 12 years ago, by S. Yajima *et al.* [1, 2]. However, despite a number of basic studies on the structure and properties of the SiC–Nicalon fibres [3–5], relationships between such structure and transient or final mechanical characteristics – and particularly the role of a microcrystalline or amorphous character of the SiC structure – are largely ignored. The level of the basic knowledge on this subject might be compared to the available knowledge on this subject, some 15 years ago, about carbon fibres.

The present study contributes to an understanding of the relationship between structure and properties of Nicalon fibres and of the structure of some experimental SiC powders; use is made, mainly, of two techniques which were hitherto of very limited use in the said domain, namely EXAFS spectrometry and very wide angle X-ray diffractometry; in addition, some ESCA and some solid state NMR spectrometry were performed in order to support the interpretations.

2. Brief recall of the "Nicalon process"

The first stage of this process involves the melt-spinning, near 290° C, under an inert atmosphere, of a composition of an organosilane polymer, the polycarbosilane (PCS), with a fairly low average molecular mass, and a carefully adjusted molecular mass distribution; the crude polymer is generally obtained through a number of chemical steps, starting from the well known monomer dichlorodimethylsilane which is first polymerized into polydimethylsilane. The obtained PCS fibres, which are exceptionally fragile, are stabilized by oxidation in air near 200° C; finally, the oxidized PCS fibres, which are infusible, are progressively "ceramized", i.e. they are more or less completely transformed into silicon carbide SiC by slowly raising the temperature, in an inert atmosphere, up to about 1300° C. The role of the longitudinal stress in the course of this ceramization process is not – or only slightly – indicated in the basic patents or papers by Yajima *et al.*

This process can obviously be compared, to the well known one for carbon fibre manufacture from an organic precursor, e.g. polyacrylonitrile (PAN) fibres. Indeed, the manufacture of the PAN precursor, here again, is followed with a stabilization step, the so-called "preoxidation", before the transformation into

0022–2461/89 $03.00 + .12

carbon fibres, which arises from a progressive pyrolysis in an inert atmosphere. However, a main difference should be noticed concerning the mechanical characteristics of the precursor fibre: in the case of PAN, one deals with a textile fibre with good tenacity and resilience; in the case of PCS, one has a fibre with exceptionally high fragility – due to the very low molecular mass (1500) – without any textile value.

3. Material and methods

3.1. Nicalon fibres

Two commercial products, of different generations, were examined:

(i) A grade 100 fibre ("NG100"), with following characteristics, as indicated by the manufacturer: σ_R(rupture stress) = 2.40 GPa (gauge length: 10 mm), E(Young's modulus) = 200 GPa, specific gravity = 2.50 g cm^{-3}, oxygen content = 16 wt %.

(ii) A grade 200 fibre ("NG200"), with the following characteristics: σ_R = 2.80($\pm$0.30) GPa, E = 200($\pm$10) GPa, specific gravity = 2.57 g cm^{-3}, oxygen content = 11 wt % and diameter (individual) = 14 μm.

3.2. Experimental powders

We started with a sample from a commercial batch of commercial PCS powder manufactured by Shinetsu which we melted and recrystallized and prepared small amounts of oxidized powder, and, from them, small amounts of "preceramized" SiC powder. Oxidation of the PCS recrystallized powder was performed in air at 190° C (3 h). Preceramization of the oxidized PCS powder was achieved in a nitrogen atmosphere by raising the temperature from 200° C up to 900° C (rate 100° C h^{-1}); then one hour at 900° C and, finally, rapid cooling to room temperature in nitrogen.

The three samples, with respective references: PCS, for initial powder, PCSO for oxidized powder and PTO for preceramized powder, had a mean granular size of 2 μm.

The specific gravity of PTO powder was measured by flotation and found to be 2.41 g cm^{-3}.

3.3. Method of preparation

Fibres are generally ground into particles with a grain size smaller than 5 μm: a vibrating grinder with cemented steel balls was used; in general some iron particles are produced during the grinding process; however, this effect is minimized after a few repeated operations on account of the formation of a thin SiC layer on the ball surface; (production of more disturbing pollution effects are observed with other "stronger" materials like tungsten carbide).

As far as EXAFS studies are concerned, the obtained powder was suspended in water in order to isolate the finer particles, which fall more slowly: the "dwell-time" for sedimentation was about 1 h for a particle volume fraction of 1 mg per 10 cm^3. The upper fraction of the liquid was then collected with a syringe and projected onto a filter holder under pressure in a closed chamber; this holder was equipped with a "millipore" membrane 1 cm in diameter. We thus obtained a uniform film made of the SiC powder. This preparation procedure is a modified version of the one used in previous EXAFS work on glass material [6].

In the case of wide-angle X-ray diffraction studies, as well as for ESCA, the as-ground powder (i.e. without decantation in water) was compacted into platelets with a surface of about 1 cm^2 and a thickness of 0.5 mm. For the NMR studies the powders were put in a cylindrical rotor of 1 cm height and 5 mm diameter.

3.4. Description of the physical methods used: equipment and mode of performance

3.4.1. EXAFS spectrometry

We performed two different types of experiments: in the first one, we measured the transmitted intensity through the sample prepared as described above; in the second one, we did a surface EXAFS type of experiment by collecting the total electron yield from the sample. It has been shown that the latter signal intensity is proportional to the absorption coefficient, while the mean free path of the electrons allows a sampling depth of about 10 to 20 nm. Such type of data collection (yield mode) was only performed on the NG200 sample, either on the powder form, or on genuine carefully aligned fibres, in order to study the surface; (of course, in the latter case, a check of the consistency of the results was also performed on the powdered SiC-whisker reference samples).

We used the "ACO" storage ring at Orsay, and the two-crystal monochromator equipped with InSb crystals [7]. The signal is detected with an ion chamber filled with 200 torr of air, in the absorption case, while the yield collection uses a classical "channeltron" equipment in the counting mode. On account of the low photon flux emitted by ACO in the energy domain 1800–2500 eV, the normalization of either the transmitted flux or the yield signal is done by a separate experiment either without sample or using a piece of copper respectively. A standard spectrum is collected within about 2 h.

The EXAFS signal is extracted from the raw absorption data using a three-region cubic spline spanning from the edge to about 300 eV beyond it. Then it is processed according to the classical way, i.e. Fourier transforming (FT) and filtering the data. Like in previous studies [8] on silicon compounds, we started our analysis as close as possible (5 to 10 eV) from the edge: this procedure allows, due to mean free path effects to visualize high order shells of crystalline systems: it was shown that multiple scattering complications have a negligible effect in such peculiar systems.

In order to extract structural parameters (distances and coordination numbers) from a given filtered shell, a least square fit procedure is applied to the experimental data using the now well known formula for EXAFS signal [9]

$$\chi(k) = \sum \frac{-N}{kR^2} \exp(-2\sigma^2 k^2) \times \exp(-R/\lambda)|f(\pi)| \sin(2kR + \Phi)$$

where N and R are the numbers and distances of one given type of atom, $f(\pi)$ and Φ are its scattering

amplitude and phase-shift, σ the disorder factor of the bond and λ the mean free path of the photoelectron. Instead using calculated values, we extracted the back-scattering amplitudes $f(\pi)$ and phase shift function Φ from model compounds of known crystallographic structures, namely crystalline SiC whiskers, and crystalline SiO_2. In such cases, the only parameters left in the fitting procedure are the interatomic distances and the coordination numbers of the studied samples.

3.4.2. X-ray diffractometry

In order to control the fibres and powders we first performed Guinier diagrams with CuKα radiation.

The X-ray diffraction patterns were obtained either from packing of SiC fibres (only for Nicalon samples) or from powders (all the samples). A conventional θ–2θ goniometer was used with the MoKα radiation. The diffracted intensities were recorded by means of a solid state detector up to K $(=(4\pi \sin \theta)/2) = 170\,nm^{-1}$. Usual corrections were applied to the intensities such as polarization and Compton background contribution which is very important at high angles for the light elements.

The Fourier transform (FT) of the interference function was calculated up to the highest possible value of k, in order to get more precision on the short and medium range order on the radial distribution function (RDF).

3.4.3. ESCA and solid state NMR spectrometry

ESCA was performed using an aluminium source and a spot size of 600 μm. The powders (2 μm grain size) were etched by argon ions prior to analysis. The analysis were conducted at "Science et Surface SA" (Lyon-Charbonnieres).

Solid state NMR was also performed on powder samples (the same powder pools from Nicalon fibres were used as for EXAFS and X-ray studies) using a Bruker CXP300 spectrometer operated at a 7 T magnetic field and a 59.6 MHz radiofrequency for the ^{29}Si nucleus and a Bruker CXP100 spectrometer operated at a 2.3 T magnetic field and a 25.2 MHz radiofrequency for the ^{13}C nucleus; the sample in the cavity was spinning at the "magic" angle (54° 44′) at 4 kHz in order to minimize line-broadening effects, according [10].

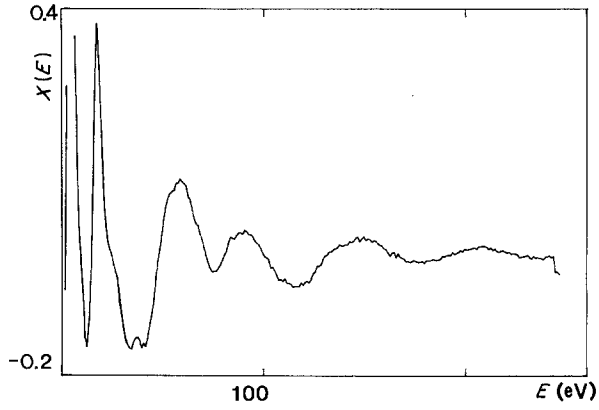

Figure 2 EXAFS data for NG200 fibre.

4. Results

4.1. EXAFS data

4.1.1. Absorption experiments

Fig. 1 compares the raw absorption spectrum of the crystalline SiC whiskers at the silicon edge and the NG200's one, while Fig. 2 represents the EXAFS signals after background extraction, and Fig. 3 the FT of those data, k^2-weighted using a Hanning window which spans from 0.17 to 0.84 nm.

Fig. 4 compares various FTs, obtained in the same mathematical conditions, for two model compounds (SiC whiskers and crystalline SiO_2) and the five samples of the present study. Notice that, because of phase shift effects, the peaks positions are shifted with respect to their crystallographic value, while the peaks amplitudes are not directly proportional to the coordination numbers: this is the reason for a comparison with model compounds.

Table I gives all the numerical values obtained from the "two-shells least square fit" procedure, limited to the two first peaks of FTs. Obviously, in the cases of SiC-whiskers and of SiO_2-quartz, these numbers are the crystallographic values we enter into the analysis. All these numbers are from absorption experiments and, therefore, are representative of the average environment of the silicon atoms in the bulk of the material. The total number of silicon neighbours has been renormalized to 4.

4.1.1.1. NG200 fibres. The closeness of the two FTs of the fibre and of the SiC whiskers, up to about 0.6 nm

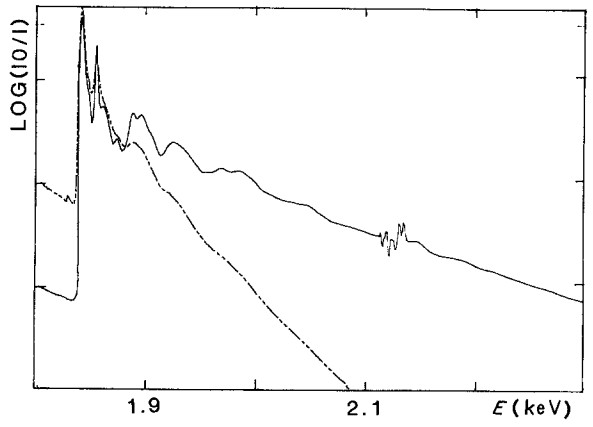

Figure 1 Absorption spectra at the Si K edge of crystalline SiC (——), and NG200 fibre (– – –).

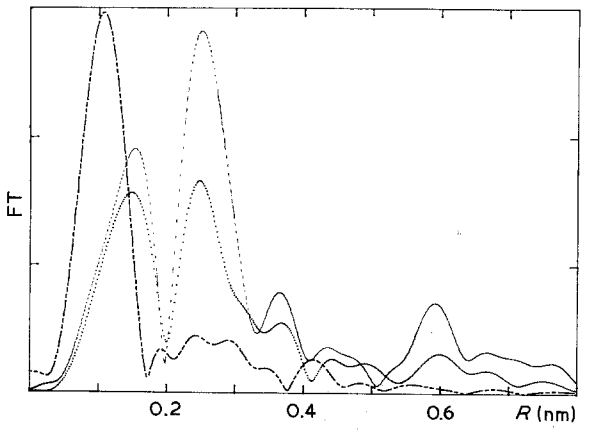

Figure 3 Fourier Transform of the EXAFS data for c-SiC (——), a-SiO_2 (– – –), and NG200 fibre (· · · ·).

TABLE I EXAFS results (interatomic distances and coordination numbers) on the various samples studied in the text

	Si–C		Si–O		Si–Si	
	N	R (nm)	N	R (nm)	N	R (nm)
SiC	4	0.189			12	0.307
SiO_2			4	0.161	4	0.306
NG200	3.85	0.186	0.15	0.162	7.3	0.305
NG100	3.2	0.19	0.8	0.162	5	0.309
PCS	2.8	0.188	1.2	0.161		
PCSO	1.75	0.188	2.25	0.161	3	0.309
PT0			3.85	0.163		

The accuracy is of about 1% for the distances, and 10% for the coordination numbers.

is an indication that this sample is made of small crystallites of SiC type, with a diamond-like structure: the existence of the eighth silicon shell at about 0.68 nm, (corrected for phase shift effects), indicates a high level of order for this sample. For fcc structure, calculations were done in literature [11] which correlate the coordination numbers of the first shells to the average size of the clusters, depending on their overall shape (spheres, cubes, platelets). In our case, only considering the fcc sublattice of silicon atoms and assuming a spherical cluster, the average coordination number of 7.3 in the first shell implies a mean diameter of 1.3–1.4 nm. This cluster then extends to the sixth shell and contains about 80 atoms. Assuming that the 30 outermost atoms have substituted one carbon bond by an oxygen one, we obtain an average first shell coordination of

$$(54 \times 4 + 30 \times 3)/84 = 3.65 \text{ carbon atoms,}$$

and

$$30/84 = 0.35 \text{ oxygen atoms.}$$

values which are not very far from the results reported in Table I.

4.1.1.2. NG100 fibres. From the FTs of Fig. 4, the decrease of crystallinity, as compared to the NG200 fibre, is evident and the same type of calculation can be performed. A coordination number of 5 means a diameter of about 0.6 nm, a central silicon atom being only surrounded, on its sublattice, by its 12 first neighbours. Assuming, as before, that these 12 outer atoms have replaced one carbon bond by an oxygen one, the mean first shell coordination number of one silicon atom becomes 3.08 carbon atom plus 0.92 oxygen atom. Once again the first and second shell results appear to be consistent with the only – oversimplified as it might be – assumption that the surface atoms of the cluster are bound to an oxygen atom.

4.1.1.3. PCS and PCSO powders. Table I indicates that the PCS powder contains quite a large amount of oxygen, which was not expected. Quite logically, the oxygen contribution increases when one moves to the PCSO powder; in the latter, one can point out the presence of Si–Si distance at 0.309 nm, a distance one might attribute to Si–O–Si or to Si–C–Si units; in the PCSO powder, the silicon network is almost equally bound to carbon and to oxygen atoms, without any evidence for crystallinity.

4.1.1.4. PTO powder. The numerical results indicate almost no Si–C distance and no middle range order.

4.1.2. Surface EXAFS results

Fig. 5 shows, in the same working conditions, the FT of yield results on the NG200 fibre, together with the absorption data.As far as the powder sample is concerned, the difference between surface and bulk data is only apparent on the first shell, which shows an increased contribution of Si–O coordination; this increase is more evident on the fibre sample, indicating a surface oxidation; however, this oxidation is probably not uniform, since there is still a strong

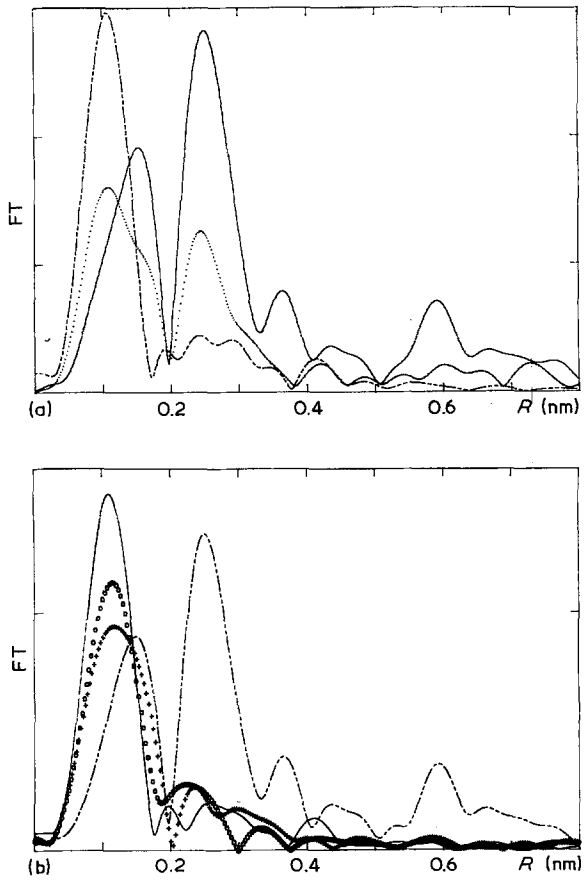

Figure 4 FT for the five samples, compared to the two standards c-SiC and c-SiO_2 (a) NG100 (· · · ·) (b) PCS (+ + +) and PCSO (o o o) powders (c) PTO powder (* * *).

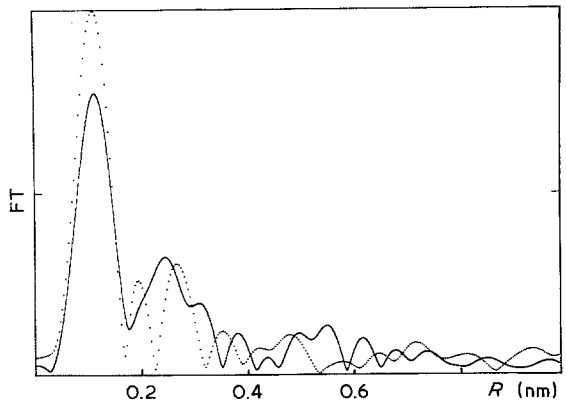

Figure 5 FT of EXAFS data recorded by total yield detection for NG200 fibre (——) and SiO_2 (····).

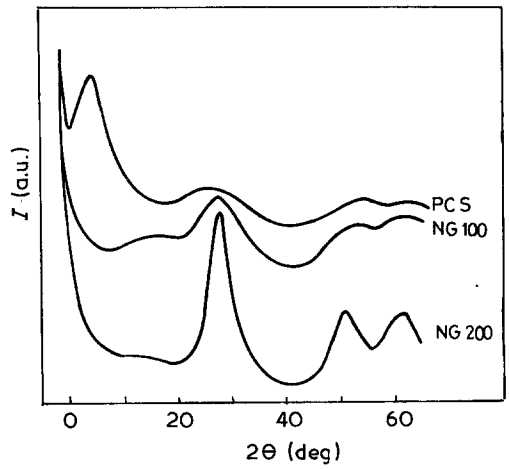

Figure 6 X-Ray diffraction pattern (up to large angles) for NG200, NG100, and PCS powders: notice the "low angle ring" for the latter.

contribution of the second Si–Si shell. The shoulder at 0.313 nm (uncorrected for phase shift effects) which was detected in the "bulk" data, is apparent, here, as a well defined peak, such distance is close to the various interatomic distances present in crystalline SiO_2, and its increase in intensity must be related to an increase of Si–O bonds present besides the Si–C ones. It therefore seems that this 0.313 nm peak is a signature of the way the SiC clusters present in the structure link together via Si–O–Si bonds.

4.2. Results of X-ray diffractometry

4.2.1. Nicalon fibres

4.2.1.1. Aspect of the diffraction patterns. The three peculiar features, besides the wide halos of all the patterns, which are characteristic of these diagrams, are a more or less pronounced small angle scattering, and the fact that interference oscillations are seen up to the large k values. Qualitatively speaking, it means that the very short range order is strong (i.e. the statistical fluctuations of the bond angles and of the distances are small), like in a molecule.

Conversely, the small angle scattering intensity and extension is the signature, in reciprocal space, of the heterogeneous character of this material, with a particles size lying between 1 and 5 nm.

The third feature is a "prepeak" near 0.12 nm, i.e. just before the first halo. So, it is likely that no long range order is to be expected.

4.2.1.2. The pairs distances. The reduced RDF of the two Nicalon fibres are shown on Fig. 8. There is a strong truncation (or termination) effect of the integration limits due to the important oscillations of the interference function at high k values. In particular the peak at 0.250 nm, which could be attributed to the O–O first distance in SiO_2, seems to be generated by the resonance of the termination effect arising from both the first and second neighbours. This was confirmed by changing the value of the higher integration limit.

All the other maxima correspond to the real pairs distances. It is surprising that all the peaks, up to 1 nm, can be interpreted as pair distances in the SiC crystallite.

From a precise measurement of the first peak position, one can derive an estimation of the bonded oxygen percentage, assuming a linear variation between the values of SiC and SiO components: one finds 15% for NG100 fibre, and 11% for NG200 fibre, which is in close agreement with values indicated by the manufacturer (see above). These figures were also confirmed by some Rutherford back scattering experiments, conducted by Dr Aigus at "Laboratoire de Physique du Solide de l'Ecole Normale Supérieure".

Since we have assumed that the peak at 0.25 nm is

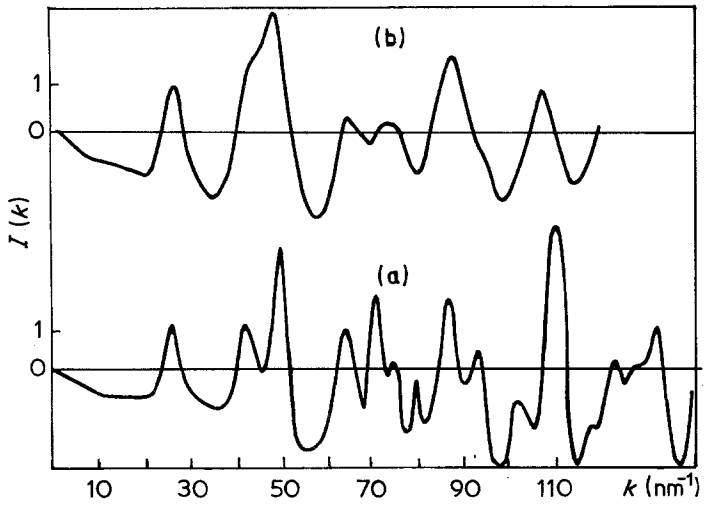

Figure 7 $I(k)$ plot for the two Nicalon fibres against k (nm^{-1}). (a) NG200 fibre, (b) NG100 fibre.

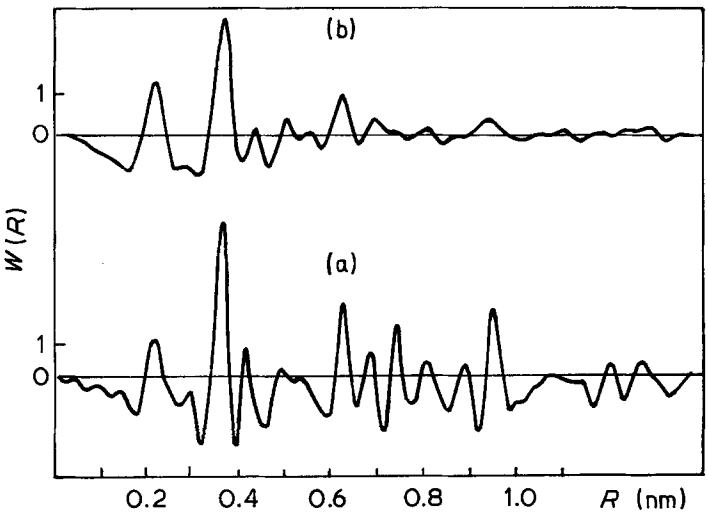

Figure 8 $W(r)$ plot against r(nm) up to 1.3 nm for Nicalon samples. (a) NG200 fibre, (b) NG100 fibre.

mainly an artifact, it means that oxygen atoms are mostly distributed as Si–O and/or C–O bonds, as in the SiO_4 tetrahedral units.

4.2.2. PCS and PCSO powders

4.2.2.1. Aspect of the diffraction pattern. A very intense ring appears at $k = 8\,\text{nm}^{-1}$ (Figs 6 to 9) for the precursor before oxidation. It is located near the small angle scattering, which suggests that is must be produced by interparticular interferences. It is known from IR and NMR studies [5] that the precursor structure is probably built, at least in part, with hexagonal cycles of alternating silicon and carbon atoms, more or less saturated by hydrogen atoms. So, individual clusters of SiC are separated from one another by hydrogen layers, which creates large fluctuations of electron density, giving rise to interparticular interferences. The distances between two clusters (which is also their diameter if they are close-packed) is derived from the formula giving the mean interparticular distances

$$x = 1.23 \times 2\pi/k_m$$

One finds 0.9 nm, i.e. about the size of two six-membered rings of SiC (Fig. 10).

The small-angle diffraction ring disappears after the "preceramization" process, i.e. for the PTO powder. This is easily interpreted, if one supposes that the hydrogen layer between SiC clusters is eliminated by high temperature treatment: so, there are no more strong electronic density fluctuations between the clusters, while they begin establishing some connection between one another. However, on account of their being randomly oriented, there is no long-range order generated by this coalescence process. The electronic density fluctuations arising from grain boundaries only generate a small angle scattering as in the case of Nicalon fibres.

4.2.2.2. The pairs distances. The medium-range order, observed in the Nicalon fibres in the 0.5–1.0 nm interval, is, here, completely absent. Besides the two first distances of the individual covalent triangles, there is just one more or less well defined distance at 0.37 nm: this corresponds to the diagonal of a six-membered ring, i.e. the second Si–C distance. An additional bump at 0.45 nm indicates that the cluster is probably made up of more than one six-membered ring, but not more than two or three deformed connected cycles. The small ripples beyond 0.5 nm are probably due to termination effects.

The PSCO powder is less ordered than the PCS one. There are also some remaining termination effects at 0.145 and 0.240 nm, which could be attributed to C–C first neighbours and O–O first neighbours in the SiO_4 tetrahedron, respectively. (However, more refinement

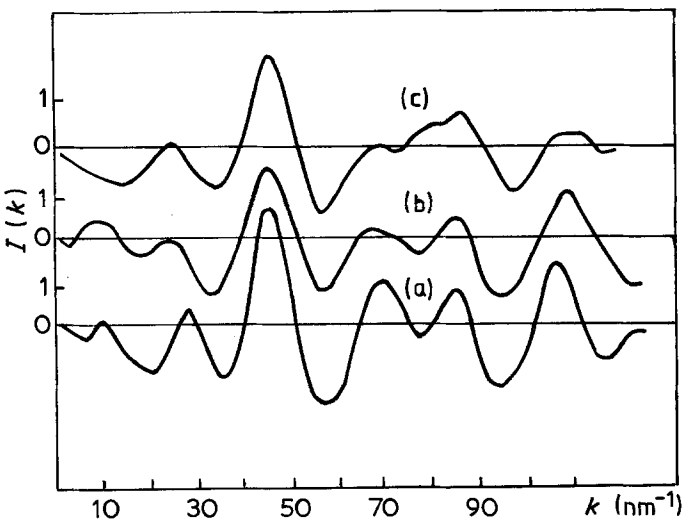

Figure 9 $I(k)$ plot against $k(\text{nm}^{-1})$ for (a) PCS powder, (b) PCSO powder and (c) PTO powder.

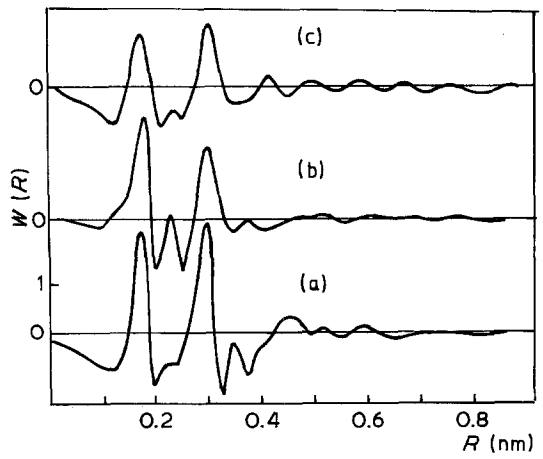

Figure 10 $W(r)$ plot against r(nm) up to 0.9 nm for (a) PCS powder, (b) PCSO powder and (c) PTO powder.

of the FT process is needed in order to eliminate the truncation ripples).

4.2.3. PTO powder

Finally, the PTO powder is a purely amorphous material, in the sense that, except the two first distances of the elementary triangle (or tetrahedron) SiO_4, there is no medium-range order, i.e. no organized connections between the Si–C covalent bonds. The high temperature treatment has eliminated hydrogen atoms, and the individual randomly oriented small clusters have coalesced, without forming neither long chains nor a two- or three-dimensional network. Oxygen atoms are probably bridging with one another, through Si–O bonds, some SiC units, thus preventing long range order developing.

4.3. Results for ESCA

4.3.1. NG100 fibre

Fig. 11 corresponds to the NG100 fibres, as far as silicon, oxygen and carbon atoms respectively are

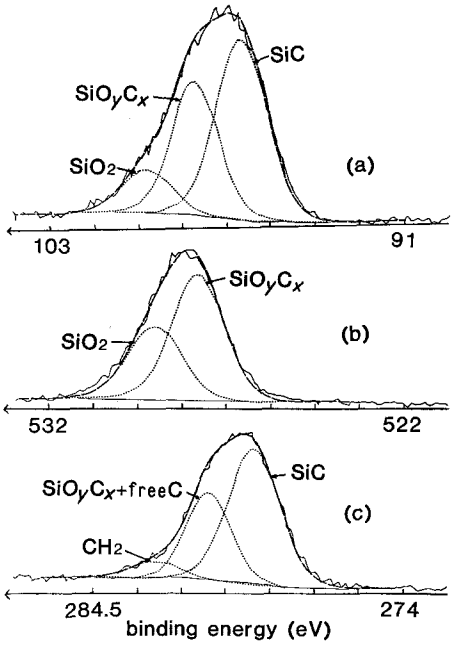

Figure 11 ESCA results for NG100 fibre. (a) silicon 2p peak, (b) oxygen 1s peak, (c) carbon 1s peak.

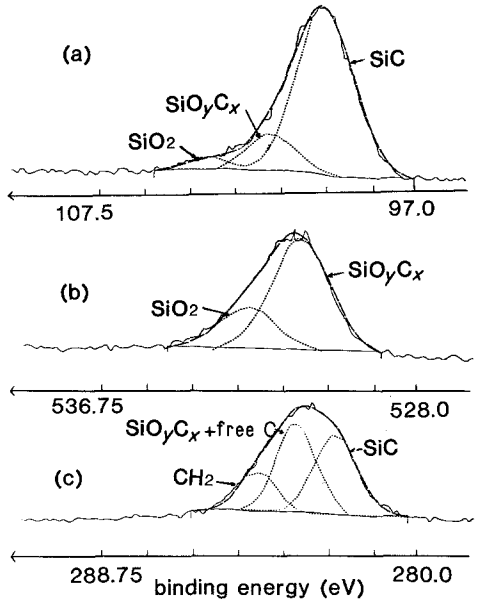

Figure 12 ESCA results for NG200 fibre. (a) silicon 2p peak, (b) oxygen 1s peak and (c) carbon 1s peak.

concerned. As far as silicon is concerned, one might decompose the peak into three components; the lower energy "sub-peak" is similar to the unique peak observed in the case of SiC whiskers, and is accordingly attributed to SiC microcrystallites; the higher energy peak may be attributed to SiO_2, on account of its energy value; finally, the intermediate peak (binding energy near 98 eV) is attributed to a compound of the form SiC_xO_y where silicon is bound both to oxygen and carbon.

As far as oxygen is concerned (Fig. 11b), one finds only two peaks rather than 3 from the experimental envelope, and they are attributed to SiO_2 for the higher energy one and to SiC_xO_y for the other. Finally, the

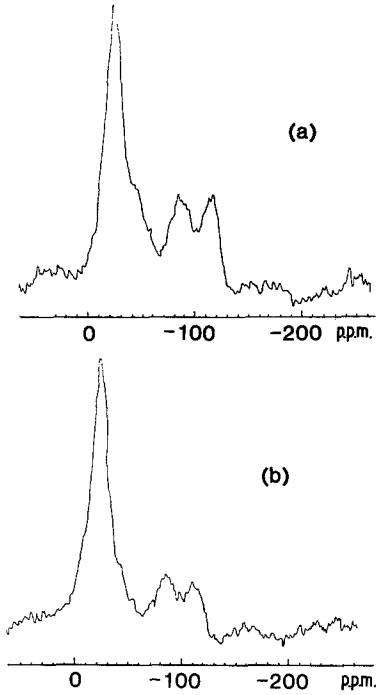

Figure 13 ^{29}Si solid state NMR referred to TMS for (a) NG100; number of scans 278, repetition time 150 sec. and (b) NG200; number of scans 120, repetition time 200 sec.

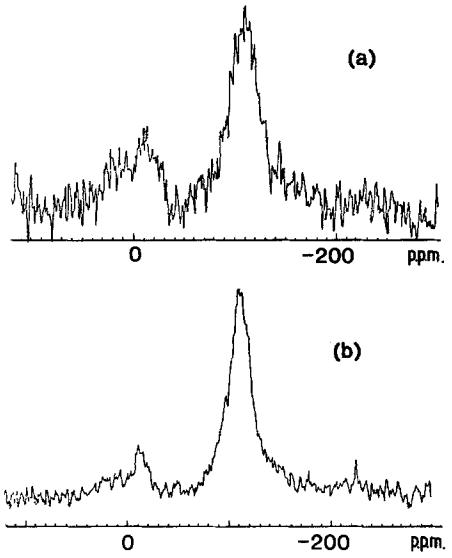

Figure 14 ^{13}C solid state NMR referred to C_6H_6 (at +129 p.p.m. of TMS) for (a) NG100; number of scans 7100, repetition time 6 sec. and (b) NG200; number of scans 9220, repetition time 5 sec.

carbon 1s curve (Fig. 11c) also seems to decompose into three components: SiC for the lower energy peak (274.5 eV): CH for the larger energy peak (282 eV), hydrogen atoms being bound to some free carbon atoms (see discussion below); the intermediate peak, in that particular case, might be attributed to the already mentioned SiC_xO_y compound, and also to a free carbon peak which is confused with the other peak (see discussion below).

4.3.2. NG200 fibres

The results are presented in Fig. 12, for silicon, oxygen and carbon atoms respectively; if one compares the results of the deconvolution programmes on the raw data, to the corresponding ones for the NG100 fibre, one notices that the peak of the SiC_xO_y component if of a lesser relative magnitude; (compare Figs 11a and 12a).

4.4. Results for NMR spectroscopy

Fig. 14 corresponds to the ^{13}C NMR spectra of sample NG100 and NG200 respectively. One notices two broad lines centered at 22 and 130 p.p.m. (referred to as TMS). The ^{13}C peak at 22 p.p.m. is very close to that of the whiskers (19 p.p.m.) and can be attributed to a CSi_4 structure; around 130 p.p.m. there is a peak which is attributed to aromatic carbon and could correspond to free carbon. Some cross-polarization experiments from ^{13}C by ^1H show no enhancement of the peaks, but rather a diminution of the intensities (more marked for the 22 p.p.m. peak) indicating that both ^{13}C species present in the fibre are very poorly protonated. The ^{13}C NMR shows evidence of CSi_4 tetrahedra and aromatic carbon clusters (free carbon).

Fig. 13 represents the ^{29}Si NMR spectra of samples NG100 and NG200 respectively. One notices four broad lines centred at −14, −32, −72 and −104 p.p.m. (referred to TMS). As compared to the NG100 fibre, the line at −32 p.p.m. for the NG200 fibre is much less intense and less well resolved; moreover the two lines at −72 and −104 p.p.m. are

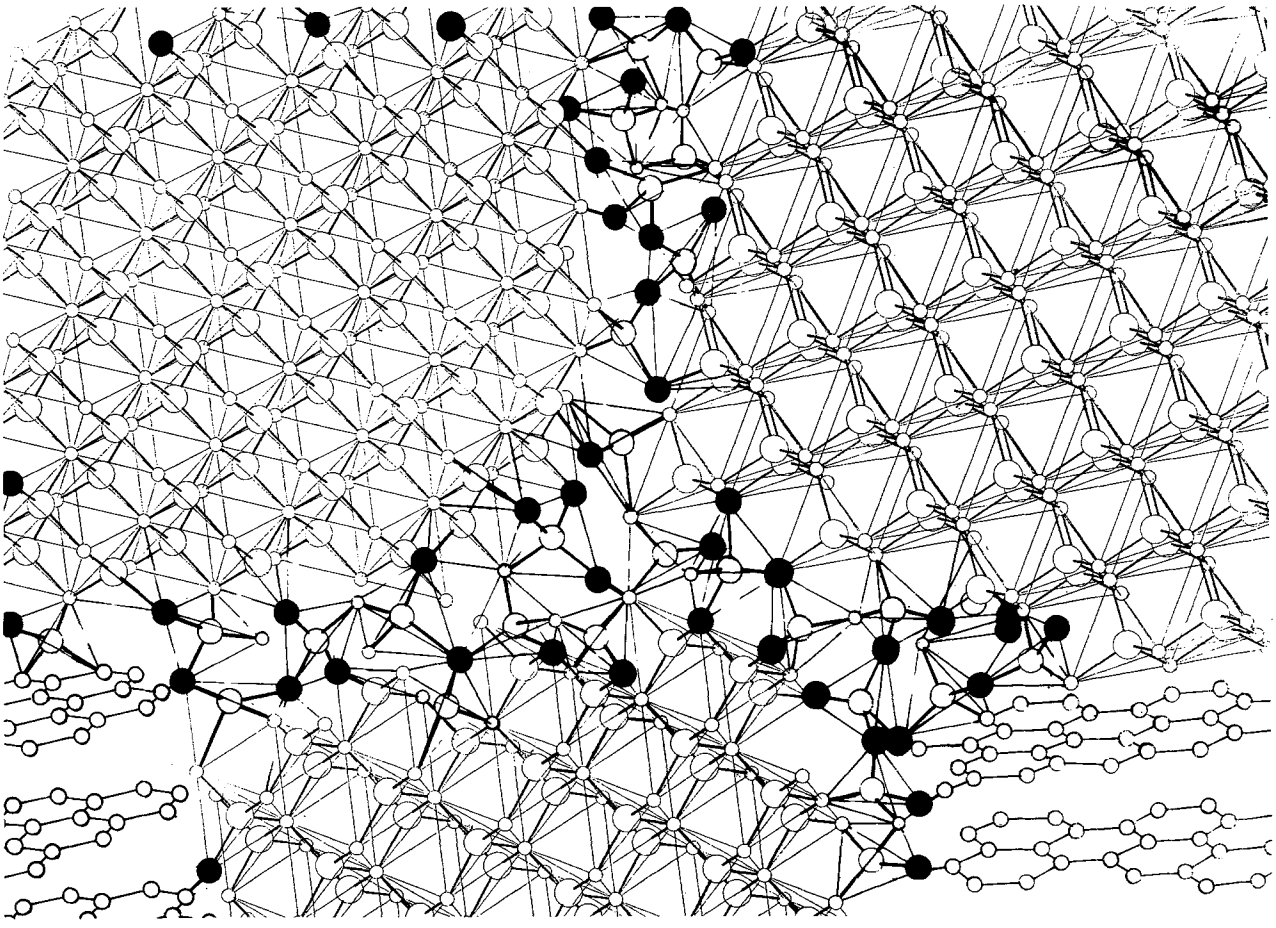

Figure 15 Model proposed for the structure of the NG200 fibre. Silicon atoms (○○○); carbon atoms (○○○); oxygen atoms (●●●).

significantly less intense. The relaxation times of all the ^{29}Si species are of the same order of magnitude and are very long (several tenths of seconds) indicating the the magnetic interaction are relatively small, but similar for all species.

The -14 p.p.m. line is close to the unique line observed in the case of SiC whiskers (this latter is at -19 p.p.m. and corresponds to silicon surrounded by four carbon atoms). Moreover the linewidth is larger for the Nicalon fibre than for the whiskers demonstrating, as expected, that the crystallization achieved is better in the latter case. For the two studied fibres the -104 p.p.m. line can be attributed to SiO_4 tetrahedra, the line at -72 p.p.m. to $SiCO_3$ tetrahedra, while the line at -32 p.p.m. could correspond to SiC_2O_2. Once can see that the species SiC_3O would give a line at about 7 p.p.m. [12], which is embedded in the SiC main peak. The intensities of the oxygenated species SiC_xO_y are larger for the NG100 fibre as expected.

5. Discussion

No extensive study of SiC fibre structure was done up to now. Nevertheless, this case is of interest in the general scheme of amorphous structures since the first X-ray patterns obtained show, through the measurement of the first halo full width at half-maximum height (FWHM), a large variation of the apparent crystal size of the coherent volume, depending on the preparation conditions of the test sample. This crystal size range extends from 1 to 3 nm, which overlaps the region where it is usually acknowledged that the transition from glassy to microcrystalline structure occurs. For example, the critical size for pure silicon lies around 2 nm; (there are no smaller microcrystals than 2 nm, the material being considered as a glass for lower sizes).

Besides the coherence volume size, derived from FWHM, one can obtain more precise information from the RDF: it is well known that the difference in short-range order between the glassy and crystalline states for silicon lies on the third pair distance of the RDF, which corresponds to the smallest distance between atoms belonging to two adjacent tetrahedra: instead of a unique peak arising from the fixed value at 60° of dihedral angle between adjacent tetrahedra, for the crystalline state, one observes a widespread continuum of distances in the glassy state.

Another point is to try and elucidate the way of how the oxygen atoms introduced during processing are distributed into the disordered material and linked to silicon and carbon atoms. EXAFS demonstrates that silicon cannot be linked to carbon atoms only and that a certain amount of Si–O bonds must be considered. This is well confirmed by ESCA and NMR, although it was not possible to obtain further informations about free carbon, as compared to those exposed in a recent paper [13]. In fact, assuming that free carbon and SiC_xO_y give quasi-identical ESCA "subpeaks", on the carbon 1s deconvolution, one could calculate free carbon content from the various stoichiometric equations arising from the three deconvoluted peaks. This, however, was not yet done, on account of the still insufficient precision of the ESCA recordings.

6. Conclusion

Although no new information was obtained about free carbon, the different investigation techniques used in the present study permit an alternative model to be proposed, as far as SiC–Nicalon fibres are concerned, to the model accepted by Yajima's followers, namely a microcrystalline fine grained fibre.

The fibre would be composed of a "continuum" of tetrahedra of two types: SiC_4 and SiC_xO_y (with $x + y = 4$). The probability of existence of domains of pure SiC_4 tetrahedra is precisely equal to the content in the SiC species in the fibre, as derived from EXAFS and WAXS analysis. On the fibre surface there is obviously a thin (some hundreds angstroms) SiO_2 layer, but the bulk of the structure is not concerned with this species. In addition, free aromatic carbon aggregates would be inserted in between the tetrahedra continuum, and themselves surrounded by hydrogen atoms. This model is represented on Fig. 15 which is a two-dimensional computer-designed drawing (free carbon was introduced more or less arbitrarily).

Another interesting conclusion is that the architecture of this continuum of tetrahedra which makes up the "mineral" structure is very close to the starting PCS architecture. In such circumstances, the so-called "organic–inorganic" transition is merely a thermal elimination of some lateral CH_3 groups, which allows for a light decrease of valence angles.

Thus for Nicalon fibres the inorganic material skeleton would be "contained" in the starting polymer. The question is to know whether the above condition, which is obviously a sufficient one to obtain valuable ceramic fibres, is also a necessary condition: the new model gives a better account for the excellent mechanical properties of Nicalon fibres than the previous model does.

This model will have to be more thoroughly quantified by ESCA and NMR studies, and examined by transmission electron microscopy, ESR spectroscopy and SAXS, as far as free carbon aggregates are concerned.

Acknowledgements

We are grateful to the operators of the ACO storage ring and those of the Compagnie Science et Surface (69260 Charbonnières France).

References

1. S. YAJIMA, K. OKAMURA and M. OMORI, *Chem. Lett.* **9** (1975) 931.
2. S. YAJIMA, K. OKAMURA, J. HAYASHI and M. OMORI, *J. Amer. Chem. Soc.* **59** (1976) 324.
3. C. H. ANDERSON and R. WARREN, "Advances in Composite Materials ICCM 3" Vol. 2 (edited by A. R. Bunsell *et al.*) Pujama (1980) p. 1129.
4. S. YAJIMA, K. OKAMURA, T. MATSUZAWA, Y. HASEGAWA and T. SHISHIDO, *Nature* **279** (1979) 706.
5. G. SIMON, Thesis Paris (1984).
6. G. N. GREAVES, A. FONTAINE, P. LAGARDE and D. RAOUX, *Nature* **293** (1981) 611.
7. A. FONTAINE, P. LAGARDE, D. RAOUX and J. M.

ESTEVA, *J. Phys. F* **9** (1979) 2143.
8. P. LAGARDE and A. M. FLANK, *J. Physique* **47** (1986) 1389.
9. P. A. LEE, P. H. CITRIN, P. EISENBERGER and B. M. KINCAID, *Rev. Mod. Phys.* **53** (1981) 769.
10. C. S. YANNONI, *Acc. Chem. Res.* **15** (1982) 201.
11. R. B. GREEGOR and F. W. LYTLE, *J. Catal.* **63** (1980) 476.
12. H. MARSMAN, "NMR Basic Principles and Progress" No. 17 (edited by P. Diehl, E. Fluck and R. Kosfeld) Springer, Berlin (1981).
13. B. CATOIRE, M. SOTTON, G. SIMON and A. BUNSELL, *Polymer* **28** (1987).

Received 19 October 1987
and accepted 17 February 1988